ATLAS PUB Note

ATL-PHYS-PUB-2018-008

29th June 2018
Minor revision: 19 February 2021

Search for scalar dark energy in $t\bar{t} + E_{\mathrm{T}}^{\mathrm{miss}}$ and mono-jet final states with the ATLAS detector

The ATLAS Collaboration

This note presents the first collider search for light scalar particles that could contribute to the accelerating expansion of the observable universe. The results are based on a re-interpretation of a search for top super-partners using the $t\bar{t} + E_{\mathrm{T}}^{\mathrm{miss}}$ signature and a search for dark matter using the mono-jet signature. The analysis uses a dataset of LHC pp collision events collected with the ATLAS detector at $\sqrt{s} = 13$ TeV corresponding to an integrated luminosity of 36.1 fb^{-1}. No significant excess over the predicted background is observed. The search allows to set the most stringent constraints on the suppression scale of conformal and disformal couplings of dark energy to standard model matter in the context of an effective field theory of dark energy.

Update 19 February 2021: a typo in the units for the exclusion limit on the L_2 operator was fixed in Fig. 4 (right) and in the text (fb was changed to pb).

ATL-PHYS-PUB-2018-008
19/02/2021

1 Introduction

The apparent accelerated expansion of the observable neighbourhood of the universe constitutes one of the biggest mysteries in cosmology and particle physics. The first evidence came from the High-Z Supernova Search Team [1] and the Supernova Cosmology Project [2], which established that distant supernovae are significantly farther from our galaxy than expected. In the context of a homogeneous and isotropic universe, this implied the existence of a repulsive force, which causes the universe to expand at an accelerated rate. The simplest explanation for this repulsive force in the context of general relativity, amounts to introducing a new type of matter which mimics a constant energy density, thus dubbed Dark Energy (DE). The existence of DE has been corroborated by precision measurements of the cosmic microwave background [3] and the large scale structure of the universe [4].

A plethora of models have been proposed in order to describe DE, ranging from modifications of general relativity to the addition of new particles beyond the Standard Model (SM) [5, 6]. Despite the abundance of models, no single prevailing model has been identified so far. Furthermore, it has been shown that models with extra fields can have the same phenomenology as modified gravity models; therefore cosmological observations alone might be unable to distinguish the two scenarios [7, 8]. Input from particle physics experiments is therefore important for elucidating the microscopic nature of DE.

Existing laboratory experiments are based on the indirect detection of DE, by searching for additional gravitational forces ("fifth forces") that would lead to deviations from the $1/r^2$ law [9, 10] or by searching for photons that may be produced by the interactions of specific DE candidates with intense magnetic fields [11, 12]. Multi-messenger astronomical observations also provide important information for understanding the nature of DE [13–15].

So far no direct search for DE has been carried out in collider experiments. The detection of DE signatures at colliders relies on the assumption of a non-zero coupling between the DE and SM fields. This arises naturally in many DE models; in particular it is an essential ingredient for the screening of fifth forces mediated by scalar DE fields [16].

Collider experiments offer a unique environment to search for the direct production of DE particles, should they exist, since they are sensitive to a multitude of signatures and therefore to a wider array of possible DE interactions with matter. DE can manifest itself in high energy particle collisions either through the modifications of electroweak precision observables induced by virtual DE particles or through the direct production of DE particles. The first mechanism has been found to yield very weak constraints on DE models [17, 18].

The direct DE production at colliders was identified as an effective way of detecting or constraining DE models, following the observations that the production of DE particles may be enhanced in final states with heavy quarks or high momentum transfers, which are not accessible by other laboratory experiments [19] and that certain type of couplings (disformal) of DE to SM matter cannot be constrained by local tests of gravity since they do not generate fifth forces [20].

This note presents a reinterpretation of the search for top super-partners using the $t\bar{t} + E_{\mathrm{T}}^{\mathrm{miss}}$ signature [21] in order to constrain conformal couplings of DE to SM matter and of the search for dark matter in the jet+$E_{\mathrm{T}}^{\mathrm{miss}}$ (mono-jet) signatures [22] to constrain disformal couplings. These searches use 36.1 fb^{-1} of pp collision data collected with the ATLAS detector at $\sqrt{s} = 13$ TeV. The ATLAS detector is described elsewhere [23].

2 Effective field theory for scalar dark energy

An Effective Field Theory (EFT) framework provides an economical way to describe DE, since it integrates out the microscopic dynamics of the DE interactions, which are completely unknown. Such a model has been developed in [19], following the framework of the so-called Horndeski theories [24], which provides the most general framework for describing DE theories with a scalar field with second order equations of motion. As such it contains as subsets many well-known specific DE models, such as quintessence [25], galileon [26], chameleon [27], symmetron [28, 29] and others.

2.1 Model details

The model [19] contains two classes of effective operators: operators which are invariant under shift symmetry $\phi \rightarrow \phi + c$, where ϕ denotes the DE scalar field, and operators which break this symmetry. Shift symmetric operators contain derivative interactions of ϕ with the SM particles, while operators that break the shift symmetry contain direct interactions of ϕ with the SM. While phenomenologically interesting, the latter is not included in this study.

There are nine shift-symmetric operators in the model, each suppressed by powers of a characteristic energy scale M according to the operator's dimensionality:

$$\mathcal{L} = \mathcal{L}_{\mathrm{SM}} + \sum_{i=1}^{9} c_i \mathcal{L}_i = \mathcal{L}_{\mathrm{SM}} + \sum_{i=1}^{9} \frac{c_i}{M_i^{(d-4)}} O_i^{(d)}, \tag{1}$$

where d is the operator's dimension and c_i are the Wilson coefficients. Operators $\mathcal{L}_1$–$\mathcal{L}_5$ correspond to interactions of the DE field with SM fields. The leading, i.e. least suppressed, operators are

$$\mathcal{L}_1 = \frac{\partial_\mu \phi \partial^\mu \phi}{M_1^4} T_\nu^\nu \tag{2}$$

$$\mathcal{L}_2 = \frac{\partial_\mu \phi \partial_\nu \phi}{M_2^4} T^{\mu\nu}, \tag{3}$$

where $T^{\mu\nu}$ is the energy-momentum tensor corresponding to the SM Lagrangian. The $\mathcal{L}_1$ operator corresponds to a derivative coupling of the DE field to the conformal anomaly, T_ν^ν, ($T_\nu^\nu = m\bar{\psi}\psi$ for a Dirac field) and is therefore proportional to the mass of the SM fermions to which DE couples. Signatures which probe DE production in association with $t\bar{t}$ are therefore the most sensitive to this type of coupling and are used in this note. The $\mathcal{L}_2$ operator involves derivatives of the SM fields and is therefore proportional to their momenta. Final states involving large momentum transfers, such as mono-jet offer the highest sensitivity to this type of coupling and are therefore exploited in this note. The $\mathcal{L}_1$ and $\mathcal{L}_2$ operators are respectively referred to as (kinetically dependent) conformal [30] and disformal.

Operators $\mathcal{L}_3$–$\mathcal{L}_5$ correspond to higher-order versions of $\mathcal{L}_1$ and $\mathcal{L}_2$. $\mathcal{L}_6$ corresponds to a (generalised) kinetic term for the DE scalar and operators $\mathcal{L}_7$–$\mathcal{L}_9$ correspond to the non-trivial galileon terms.

In this note, only $\mathcal{L}_1$ and $\mathcal{L}_2$ are considered. Due to the absence of terms allowing the decay of the DE scalars to SM particles, the DE particles (ϕ) are considered stable and they escape the detector producing a missing energy signature ($E_{\mathrm{T}}^{\mathrm{miss}}$).

Representative Feynman diagrams corresponding to the $\mathcal{L}_1$ and $\mathcal{L}_2$ operators for the $t\bar{t}+E_{\mathrm{T}}^{\mathrm{miss}}$ and mono-jet signatures are shown in Fig. 1.

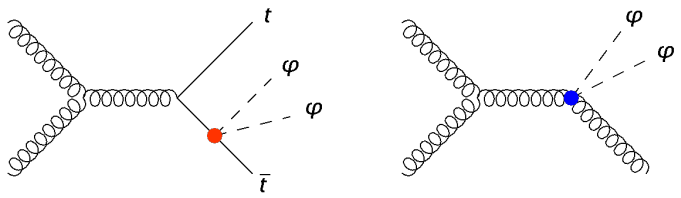

Figure 1: Feynman diagrams corresponding to the $t\bar{t} + E_{\mathrm{T}}^{\mathrm{miss}}$ (left) and mono-jet (right) final states. The red vertex corresponds to the $\mathcal{L}_1$ operator and the blue vertex corresponds to $\mathcal{L}_2$.

2.2 Event generation

The Lagrangian (1) has been implemented in the MadGraph5_aMC@NLO generator version 2.6.1 [31]. For the $t\bar{t} + E_{\mathrm{T}}^{\mathrm{miss}}$ final state a sample corresponding to the process $pp \to t\bar{t}\phi\phi$ is generated, fixing the Wilson coefficient $c_1 = 1$ and setting all other Wilson coefficients to zero, while for the mono-jet final state a sample corresponding to the process $pp \to j\phi\phi$ is generated fixing $c_2 = 1$ and setting all other Wilson coefficients to zero. In this way the upper limit on the cross-section can be expressed as a function of a single parameter, M.

Matrix elements are calculated in the 4-flavour scheme at leading order (LO) in QCD, vetoing electroweak contributions and considering only one insertion of a $\mathcal{L}_1$ or $\mathcal{L}_2$ operator in each diagram. The latter guarantees that the amplitude scales as M^{-4}, for all values of M and therefore M is just a parameter that controls the total cross-section, with the differential distributions for the signal process being independent of M. The renormalisation and factorisation scales are set to $\mu = \frac{1}{2}\sum_i m_{T,i}$, where i runs over all particles in the final state. The LO PDF set NNPDF 3.0 [32] with $\alpha_s = 0.13$ is used in the matrix element calculation. The parton shower and hadronisation are simulated using Pythia 8.212 [33] using the A14 set of tuned parameters [34] with the LO NNPDF 2.3 PDF set with $\alpha_s = 0.13$ [32].

In order to reproduce the correct equation of state for dark energy, scalar fields should have a very small mass $m_\phi = O(H_0) \sim 10^{-42}$ GeV [35]. The mass of the scalar DE field is fixed in the sample generation to $m_\phi = 0.1$ GeV [19]. The production cross-section and kinematics are in this case independent of m_ϕ.

For the $t\bar{t}\phi\phi$ sample an event selection is applied at truth level, selecting events with at least 1 lepton with $p_T > 20$ GeV and $|\eta| < 2.8$ and $E_{\mathrm{T}}^{\mathrm{miss}} > 60$ GeV or requiring $E_{\mathrm{T}}^{\mathrm{miss}} > 150$ GeV. The efficiency of this selection is 87%. For the $j\phi\phi$ sample an event selection requiring $E_{\mathrm{T}}^{\mathrm{miss}} > 150$ GeV is applied at truth level. This selection is fully efficient.

3 Event selection

The sensitivity of the search for DE in the $t\bar{t} + E_{\mathrm{T}}^{\mathrm{miss}}$ final state was estimated employing the event selections used in the search for dark matter produced in association with a $t\bar{t}$ pair [36] and in the search for stop quarks [21, 37, 38]. The latter was found to yield better exclusion limits and is therefore used in the following.

The $t\bar{t} + E_{\mathrm{T}}^{\mathrm{miss}}$ final state can be split into three channels according to the decays of the W-bosons from the top-quark decays: 0-lepton, where both W bosons decay hadronically, 1-lepton, where one of the

two W-bosons decays into leptons and 2-lepton where both W-bosons decay into leptons[1]. The 2-lepton channel has been found to have significantly smaller sensitivity due to the smaller branching ratio of $W \rightarrow \ell\nu$. The 0 and 1-lepton have similar expected sensitivities, with the 0-lepton being slightly more sensitive and therefore used in this note.

The event selection[2] for the 0-lepton $t\bar{t} + E_{\mathrm{T}}^{\mathrm{miss}}$ channel is comprised of three signal regions as shown in Table 1 [21].

Variable	Region		
	SRA_TT	SRA_TW	SRA_T0
N^{jet}	≥ 4 within $\lvert\eta\rvert < 2.7$		
$N^{\text{b-jet}}$	≥ 2		
P_T^{jet}	$> 80, 80, 40, 40$ GeV		
$m^0_{\mathrm{jet},R=1.2}$	> 120 GeV		
$m^1_{\mathrm{jet},R=1.2}$	> 120 GeV	$[60, 120]$ GeV	< 60 GeV
$m_T^{b,\mathrm{min}}$	> 200 GeV		
$N_{b-\mathrm{jet}}$	≥ 2		
τ-veto	yes		
$\lvert\Delta\phi(\mathrm{jet}^{0,1,2}, \mathbf{p}_T^{\mathrm{miss}})\rvert$	> 0.4		
$m^0_{\mathrm{jet},R=0.8}$	> 60 GeV		
$\Delta R(b,b)$	> 1	-	
$m_{T2}^{\chi^2}$	> 400 GeV	> 400 GeV	> 500 GeV
$E_{\mathrm{T}}^{\mathrm{miss}}$	> 400 GeV	> 500 GeV	> 550 GeV

Table 1: Signal region definition for the 0-lepton $t\bar{t} + E_{\mathrm{T}}^{\mathrm{miss}}$ search. The variables are defined in [21].

The search for DE in the mono-jet final state employs the event selection developed for the search for dark matter using the mono-jet signature [22]. The event selection criteria are listed in Table 2. Events

$E_{\mathrm{T}}^{\mathrm{miss}} > 250$ GeV
leading jet $p_T > 250$ GeV and $\lvert\eta\rvert < 2.4$
≤ 4 selected jets with $P_T > 30$ GeV and $\lvert\eta\rvert < 2.8$
$\Delta\phi\left(jet, \vec{p}_T^{miss}\right) > 0.4$ for all selected jets
no identified electron with $p_T > 20$ GeV
no identified muon with $p_T > 10$ GeV

Table 2: Event selection criteria for the mono-jet search.

satisfying the above criteria are binned in $E_{\mathrm{T}}^{\mathrm{miss}}$, using bin widths of 50 GeV for $250 < E_{\mathrm{T}}^{\mathrm{miss}} < 400$ GeV, 100 GeV for $400 < E_{\mathrm{T}}^{\mathrm{miss}} < 1000$ GeV and a single bin for events with $E_{\mathrm{T}}^{\mathrm{miss}} > 1000$ GeV.

[1] Here only electrons and muons are considered as leptons.

[2] For the definition of the objects used in the event selection see [21] for the $t\bar{t} + E_{\mathrm{T}}^{\mathrm{miss}}$ analysis and [22] for the mono-jet analysis.

4 Uncertainties

The theoretical uncertainties for the DE signal are estimated using a variation of the renormalisation and factorisation scales by a factor of two, as well as from the combined PDF+α_s uncertainties, which are estimated using the PDF4LHC prescription [39].

The uncertainties are split into two components: cross-section uncertainties, that only affect the overall normalisation of the signal and acceptance uncertainties, that depend on the specific kinematic selections applied. The latter are incorporated into the profile likelihood fit.

The cross-section uncertainties for the $pp \to t\bar{t}\phi\phi$ process involving the $\mathcal{L}_1$ operator are $^{+44}_{-28}$% (scale) $\oplus$ 39% (PDF) $\oplus$ 8% (α_s) $= ^{+59}_{-48}$ %. The acceptance uncertainties are 1% (scale) $\oplus$ 12% PDF $\oplus$ 1% (α_s) = 12% in all signal regions.

For the $pp \to j\phi\phi$ process involving the $\mathcal{L}_2$ operator, the cross-section uncertainties are $^{+39}_{-26}$% (scale) $\oplus$ 25% (PDF) $\oplus$ 4% (α_s) $= ^{+46}_{-36}$ %. The acceptance uncertainties depend on the $E_{\mathrm{T}}^{\mathrm{miss}}$ value, ranging from 10% at low $E_{\mathrm{T}}^{\mathrm{miss}}$ values to 30% at high $E_{\mathrm{T}}^{\mathrm{miss}}$, and are also dominated by the PDF uncertainties.

The uncertainties due to background modelling, detector systematics and data statistics are incorporated into the statistical analysis as nuisance parameters, as described in [21, 22].

5 Validity of the EFT approximation and truncation procedure

The operators that describe the interactions of the DE scalar field are obtained by an expansion in the suppression scale M and are therefore valid only in the regime where the momentum transfer is $Q_{\mathrm{tr}} \ll M$. In practice, it is assumed that the EFT approximation is valid for events where $Q_{\mathrm{tr}} < g_* M$ where g_* is a number that depends on the details of the UV completion of the model and should satisfy $g_* < 4\pi$, in order for the couplings to be in the perturbative regime [40].

Since the UV completion of the DE EFT model are unknown, a conservative approach for the evaluation of the momentum transfer amounts to using the partonic center-of-mass energy [41, 42]. This gives

$$Q_{\mathrm{tr}} = \sqrt{\hat{s}} \equiv \sqrt{\left(\sum_i p_i\right)^2} < g_* M, \tag{4}$$

where i runs over all the partons in the final state, as a condition which should be fulfilled in order for the EFT to be valid.

For events that do not satisfy Eq. 4, the iterative rescaling procedure developed in [42] is applied in order to rescale the EFT limits. The procedure amounts to iteratively estimating the fraction of events R_i that satisfy the EFT validity criterion and rescaling the limit with

$$M_{\mathrm{rescaled}} = \prod_i R_i^{1/8} M. \tag{5}$$

until the fraction of valid events reaches 0 or 1. The exponent 1/8 originates from the fact that $\sigma \propto M^{-1/8}$.

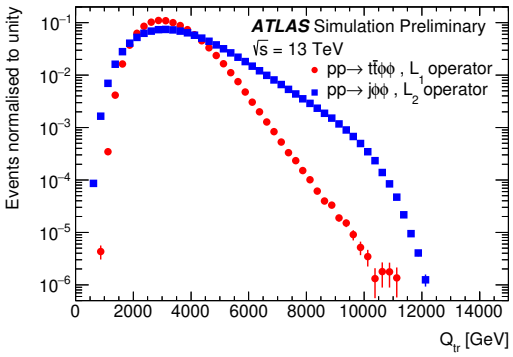

Figure 2: Q_{tr} distribution for the $t\bar{t}\phi\phi$ final state involving the $\mathcal{L}_1$ operator and for the $j\phi\phi$ final state involving the $\mathcal{L}_2$ operator after applying the respective event selection criteria.

The evaluation of the rescaled limits relies on the Q_{tr} distribution, which is evaluated at truth level after applying the analysis selection criteria described in the previous section. The Q_{tr} distributions for the $t\bar{t}\phi\phi$ and $j\phi\phi$ final states are shown in Fig. 2.

6 Results

In order to test for the presence of a DE signal, the signal and background simulated event samples are simultaneously fitted to data using a binned maximum-likelihood approach based on the RooStats [43, 44] and HistFitter [45] frameworks.

For the $t\bar{t} + E_{\mathrm{T}}^{\mathrm{miss}}$ final state the expected signal and background yield is fitted to the observed data in the three signal regions described in section 3. For the mono-jet final state the signal and background templates for the $E_{\mathrm{T}}^{\mathrm{miss}}$ spectrum are fitted to the observed data.

The $m_{T2}^{\chi^2}$ and $E_{\mathrm{T}}^{\mathrm{miss}}$ distributions for the SM background predictions after the fit to data in the $t\bar{t} + E_{\mathrm{T}}^{\mathrm{miss}}$ and mono-jet final states respectively are shown in Fig. 3.

As reported in the original publications [21, 22], no significant excess over the background prediction is observed. An upper limit at the 95% CL is set on the $pp \to t\bar{t}\phi\phi$ production cross-section involving the $\mathcal{L}_1$ operator and on the $pp \to j\phi\phi$ production cross-section involving the $\mathcal{L}_2$ operator. The limit is evaluated using the CLs method [46] and the profile-likelihood-ratio test statistic using the asymptotic approximation [47].

The upper limit on the cross-section is found to be 26 fb for $\mathcal{L}_1$ and 230 fb for $\mathcal{L}_2$, which can be translated to a lower limit on the EFT suppression scale using the fact that $\sigma \propto M^{-1/8}$. The expected and observed limits on M with the 1 and 2σ uncertainties are shown in Table 3. The corresponding exclusion plot is shown in Fig. 4.

The limit on the $\{g_*, M\}$ plane, after applying the EFT validity criterion (Eq. 4) is shown in Fig. 5.

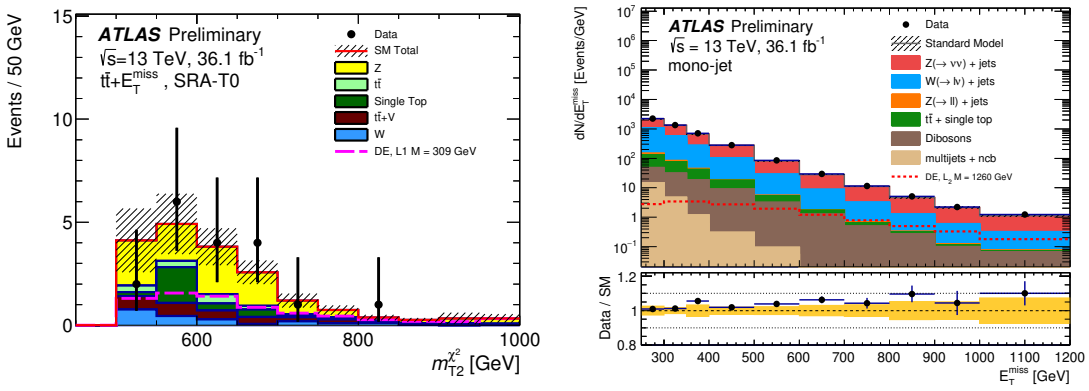

Figure 3: *Left*: The $m_{T2}^{\chi^2}$ distribution for the SM background predictions after the background-only fit to data in the SRA_T0 region of the 0-lepton $t\bar{t} + E_{\mathrm{T}}^{\mathrm{miss}}$ channel [21]. The DE signal for the $\mathcal{L}_1$ operator corresponding to the observed lower limit on the suppression scale $M = 309$ GeV is overlaid. *Right*: The $E_{\mathrm{T}}^{\mathrm{miss}}$ distribution for the SM background predictions after the background-only fit to data in the mono-jet final state [22]. The DE signal for the $\mathcal{L}_2$ operator corresponding to the observed lower limit on the suppression scale $M = 1260$ GeV is overlaid.

Channel	Operator	Lower limits on M [GeV]					
		Observed	Expected	$+2\sigma$	$+1\sigma$	-1σ	-2σ
$t\bar{t} + E_{\mathrm{T}}^{\mathrm{miss}}$	$\mathcal{L}_1$	309^{+19}_{-24}	313	284	299	326	338
Mono-jet	$\mathcal{L}_2$	1260^{+50}_{-60}	1350	1200	1280	1400	1450

Table 3: Lower limits on the suppression scale M (in GeV) for the $\mathcal{L}_1$ operator from the 0-lepton $t\bar{t} + E_{\mathrm{T}}^{\mathrm{miss}}$ search and for the $\mathcal{L}_2$ operator from the mono-jet search. The errors on the observed limit correspond to the uncertainty on the signal production cross-section. The limits quoted here are not rescaled to take into account the EFT validity criterion.

7 Summary and conclusions

This note presented the first collider search for light scalar particles with conformal and disformal couplings to SM matter. The results are obtained by a reinterpretation of the search for supersymmetric top partners in the 0-lepton $t\bar{t} + E_{\mathrm{T}}^{\mathrm{miss}}$ final state [21] and of the search for dark matter in the mono-jet final state [22] using a dataset of 36.1 fb^{-1} of pp collisions, which was collected by the ATLAS experiment at $\sqrt{s} = 13$ TeV.

The results were interpreted in the context of an EFT model of scalar dark energy, setting constraints on the production cross-section or equivalently on the EFT suppression scale of the conformal and disformal couplings generated by the two lowest dimension operators of the theory.

The $t\bar{t} + E_{\mathrm{T}}^{\mathrm{miss}}$ analysis yields the most stringent constraints on the conformal operator $\mathcal{L}_1$. As shown in Fig. 5, the $t\bar{t} + E_{\mathrm{T}}^{\mathrm{miss}}$ search is not yet sensitive to weakly coupled models, due to the high momentum transfers involved in the production of the top quarks, which are close to the exclusion limit.

The mono-jet analysis yields the most stringent constraints on the disformal operator $\mathcal{L}_2$. Due to the absence of heavy particles in the final state, the region of EFT validity for the mono-jet search is larger, with the constraints extending to lower values of the effective coupling.

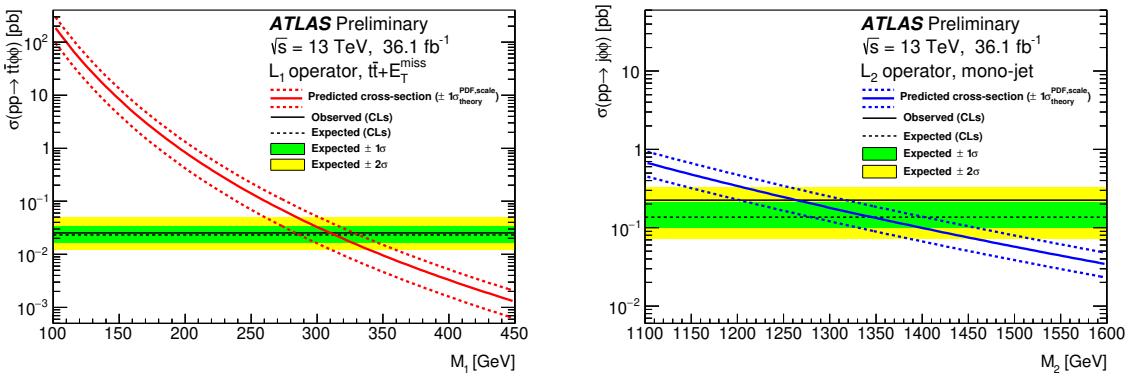

Figure 4: Exclusion plots for $\mathcal{L}_1$ (left) and $\mathcal{L}_2$ (right) from the $t\bar{t} + E_{\mathrm{T}}^{\mathrm{miss}}$ and mono-jet channels respectively, without taking into account the EFT validity criterion. The errors on the predicted cross-sections correspond to the scale and PDF uncertainties.

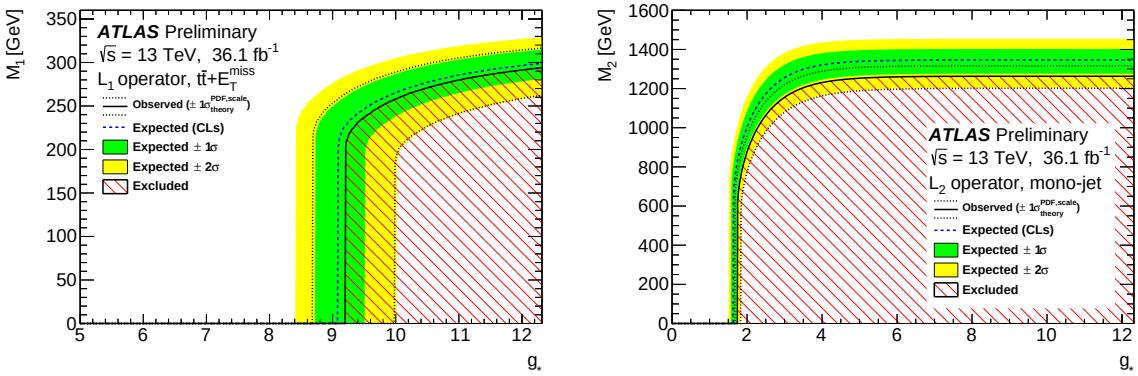

Figure 5: Exclusion plots for $\mathcal{L}_1$ (left) and $\mathcal{L}_2$ (right) on the $\{g_*, M\}$ plane, after rescaling to take into account the EFT validity criterion.

These results improve upon the constraints on the disformal operator from astrophysical probes and non-collider experiments by several orders of magnitude [48] and also represent a significant improvement over the limits obtained by a similar re-interpretation of ATLAS and CMS results that made use of a smaller dataset at $\sqrt{s} = 8$ TeV [19].

References

[1] A. G. Riess et al., *Observational evidence from supernovae for an accelerating universe and a cosmological constant*, Astron. J. **116** (1998) 1009, arXiv: astro-ph/9805201 [astro-ph].

[2] S. Perlmutter et al., *Measurements of Omega and Lambda from 42 high redshift supernovae*, Astrophys. J. **517** (1999) 565, arXiv: astro-ph/9812133 [astro-ph].

[3] Planck Collaboration, *Planck 2015 results. XIII. Cosmological parameters*, Astronomy & Astrophysics **594**, A13 (2016) A13, arXiv: 1502.01589.

[4] S. Alam et al., *The Eleventh and Twelfth Data Releases of the Sloan Digital Sky Survey: Final Data from SDSS-III*, The Astrophysical Journal Supplement Series **219**, 12 (2015) 12, arXiv: 1501.00963 [astro-ph.IM].

[5] A. Joyce, L. Lombriser and F. Schmidt, *Dark Energy Versus Modified Gravity*, Ann. Rev. Nucl. Part. Sci. **66** (2016) 95, arXiv: 1601.06133 [astro-ph.CO].

[6] T. Clifton, P. G. Ferreira, A. Padilla and C. Skordis, *Modified Gravity and Cosmology*, Phys. Rept. **513** (2012) 1, arXiv: 1106.2476 [astro-ph.CO].

[7] M. Kunz and D. Sapone, *Dark Energy versus Modified Gravity*, Phys. Rev. Lett. **98** (2007) 121301, arXiv: astro-ph/0612452 [astro-ph].

[8] M. Kunz, *The dark degeneracy: On the number and nature of dark components*, Phys. Rev. **D80** (2009) 123001, arXiv: astro-ph/0702615 [astro-ph].

[9] D. J. Kapner et al., *Tests of the gravitational inverse-square law below the dark-energy length scale*, Phys. Rev. Lett. **98** (2007) 021101, arXiv: hep-ph/0611184 [hep-ph].

[10] P. Hamilton et al., *Atom-interferometry constraints on dark energy*, Science **349** (2015) 849, arXiv: 1502.03888 [physics.atom-ph].

[11] V. Anastassopoulos et al., *Search for chameleons with CAST*, Phys. Lett. **B749** (2015) 172, arXiv: 1503.04561 [astro-ph.SR].

[12] J. H. Steffen et al., *Laboratory constraints on chameleon dark energy and power-law fields*, Phys. Rev. Lett. **105** (2010) 261803, arXiv: 1010.0988 [astro-ph.CO].

[13] B. P. Abbott et al., *Tests of general relativity with GW150914*, Phys. Rev. Lett. **116** (2016) 221101, arXiv: 1602.03841 [gr-qc].

[14] B. P. Abbott et al., *GW170817: Observation of Gravitational Waves from a Binary Neutron Star Inspiral*, Phys. Rev. Lett. **119** (2017) 161101, arXiv: 1710.05832 [gr-qc].

[15] B. P. Abbott et al., *Multi-messenger Observations of a Binary Neutron Star Merger*, Astrophys. J. **848** (2017) L12, arXiv: 1710.05833 [astro-ph.HE].

[16] A. Joyce, B. Jain, J. Khoury and M. Trodden, *Beyond the Cosmological Standard Model*, Phys. Rept. **568** (2015) 1, arXiv: 1407.0059 [astro-ph.CO].

[17] P. Brax, C. Burrage, A.-C. Davis, D. Seery and A. Weltman, *Collider constraints on interactions of dark energy with the Standard Model*, JHEP **09** (2009) 128, arXiv: 0904.3002 [hep-ph].

[18] P. Brax, C. Burrage, A.-C. Davis, D. Seery and A. Weltman, *Higgs production as a probe of Chameleon Dark Energy*, Phys. Rev. **D81** (2010) 103524, arXiv: 0911.1267 [hep-ph].

[19] P. Brax, C. Burrage, C. Englert and M. Spannowsky, *LHC Signatures Of Scalar Dark Energy*, Phys. Rev. **D94** (2016) 084054, arXiv: 1604.04299 [hep-ph].

[20] P. Brax, C. Burrage and C. Englert, *Disformal dark energy at colliders*, Phys. Rev. **D92** (2015) 044036, arXiv: 1506.04057 [hep-ph].

[21] ATLAS collaboration, *Search for a scalar partner of the top quark in the jets plus missing transverse momentum final state at $\sqrt{s}$=13 TeV with the ATLAS detector*, JHEP **12** (2017) 085, arXiv: 1709.04183 [hep-ex].

[22] ATLAS collaboration, *Search for dark matter and other new phenomena in events with an energetic jet and large missing transverse momentum using the ATLAS detector*, JHEP **01** (2018) 126, arXiv: 1711.03301 [hep-ex].

[23] ATLAS Collaboration, *The ATLAS Experiment at the CERN Large Hadron Collider*, JINST **3** (2008) S08003.

[24] G. W. Horndeski, *Second-order scalar-tensor field equations in a four-dimensional space*, International Journal of Theoretical Physics **10** (1974) 363, ISSN: 1572-9575, URL: https://doi.org/10.1007/BF01807638.

[25] R. R. Caldwell, R. Dave and P. J. Steinhardt, *Cosmological imprint of an energy component with general equation of state*, Phys. Rev. Lett. **80** (1998) 1582, arXiv: astro-ph/9708069 [astro-ph].

[26] A. Nicolis, R. Rattazzi and E. Trincherini, *The Galileon as a local modification of gravity*, Phys. Rev. **D79** (2009) 064036, arXiv: 0811.2197 [hep-th].

[27] J. Khoury and A. Weltman, *Chameleon cosmology*, Phys. Rev. D **69** (4 2004) 044026, URL: https://link.aps.org/doi/10.1103/PhysRevD.69.044026.

[28] K. A. Olive and M. Pospelov, *Environmental dependence of masses and coupling constants*, Phys. Rev. **D77** (2008) 043524, arXiv: 0709.3825 [hep-ph].

[29] K. Hinterbichler and J. Khoury, *Symmetron Fields: Screening Long-Range Forces Through Local Symmetry Restoration*, Phys. Rev. Lett. **104** (2010) 231301, arXiv: 1001.4525 [hep-th].

[30] P. Brax and P. Valageas, *Goldstone models of modified gravity*, Phys. Rev. **D95** (2017) 043515, arXiv: 1611.08279 [astro-ph.CO].

[31] J. Alwall et al., *The automated computation of tree-level and next-to-leading order differential cross sections, and their matching to parton shower simulations*, JHEP **07** (2014) 079, arXiv: 1405.0301 [hep-ph].

[32] NNPDF Collaboration, R. D. Ball et al., *Parton distributions for the LHC Run II*, JHEP **04** (2015) 040, arXiv: 1410.8849 [hep-ph].

[33] T. Sjöstrand et al., *An Introduction to PYTHIA 8.2*, Comput. Phys. Commun. **191** (2015) 159, arXiv: 1410.3012 [hep-ph].

[34] ATLAS Collaboration, *ATLAS Pythia 8 tunes to 7 TeV data*, ATL-PHYS-PUB-2014-021, 2014, URL: https://cds.cern.ch/record/1966419.

[35] P. Brax, *What makes the Universe accelerate? A review on what dark energy could be and how to test it*, Reports on Progress in Physics **81** (2018) 016902, URL: http://stacks.iop.org/0034-4885/81/i=1/a=016902.

[36] ATLAS collaboration, *Search for dark matter produced in association with bottom or top quarks in $\sqrt{s}$ = 13 TeV pp collisions with the ATLAS detector*, Eur. Phys. J. **C78** (2018) 18, arXiv: 1710.11412 [hep-ex].

[37] ATLAS collaboration, *Search for top-squark pair production in final states with one lepton, jets, and missing transverse momentum using 36 fb^{-1} of $\sqrt{s}$ = 13 TeV pp collision data with the ATLAS detector*, (2017), arXiv: 1711.11520 [hep-ex].

[38] ATLAS collaboration, *Search for direct top squark pair production in final states with two leptons in $\sqrt{s}$ = 13 TeV pp collisions with the ATLAS detector*, Eur. Phys. J. **C77** (2017) 898, arXiv: 1708.03247 [hep-ex].

[39] J. Butterworth et al., *PDF4LHC recommendations for LHC Run II*, J. Phys. **G43** (2016) 023001, arXiv: 1510.03865 [hep-ph].

[40] G. Busoni, A. De Simone, E. Morgante and A. Riotto, *On the Validity of the Effective Field Theory for Dark Matter Searches at the LHC*, Phys. Lett. **B728** (2014) 412, arXiv: 1307.2253 [hep-ph].

[41] C. Englert and M. Spannowsky, *Effective Theories and Measurements at Colliders*, Phys. Lett. **B740** (2015) 8, arXiv: 1408.5147 [hep-ph].

[42] D. Abercrombie et al., *Dark Matter Benchmark Models for Early LHC Run-2 Searches: Report of the ATLAS/CMS Dark Matter Forum*, (2015), arXiv: 1507.00966 [hep-ex].

[43] L. Moneta, K. Cranmer, G. Schott and W. Verkerke, 'The RooStats project', *Proceedings of the 13th International Workshop on Advanced Computing and Analysis Techniques in Physics Research. February 22-27, 2010, Jaipur, India. http://acat2010.cern.ch/. Published online at <A href="http://pos.sissa.it/cgi-bin/reader/conf.cgi?confid=93">http://pos.sissa.it/cgi-bin/reader/conf.cgi?confid=93</A>, id.57*, 2010 57, arXiv: 1009.1003 [physics.data-an].

[44] W. Verkerke and D. Kirkby, *The RooFit toolkit for data modeling*, ArXiv Physics e-prints (2003), eprint: physics/0306116.

[45] M. Baak et al., *HistFitter software framework for statistical data analysis*, Eur. Phys. J. **C75** (2015) 153, arXiv: 1410.1280 [hep-ex].

[46] A. L. Read, *Presentation of search results: the CL s technique*, Journal of Physics G: Nuclear and Particle Physics **28** (2002) 2693, URL: http://stacks.iop.org/0954-3899/28/i=10/a=313.

[47] G. Cowan, K. Cranmer, E. Gross and O. Vitells, *Asymptotic formulae for likelihood-based tests of new physics*, Eur. Phys. J. **C71** (2011) 1554, [Erratum: Eur. Phys. J.C73,2501(2013)], arXiv: 1007.1727 [physics.data-an].

[48] P. Brax and C. Burrage, *Constraining Disformally Coupled Scalar Fields*, Phys. Rev. **D90** (2014) 104009, arXiv: 1407.1861 [astro-ph.CO].